Boletim de Geociências da Petrobras

Identification of the Pre-Alagoas Unconformity through real-time fluorescence and X-Ray diffraction analyses of drilling cuttings

Identificação da Discordância Pré-Alagoas por meio de análises em tempo real de fluorescência e difração de Raios-X em amostras de calha

[1]**Filipe Vidal**, [2]**Jean Carlos de Amorim**
[1]Petrobras, Rio de Janeiro, Rio de Janeiro, Brazil, filipe.vidal@petrobras.com.br (Autor correspondente)
[2]Petrobras, Rio de Janeiro, Rio de Janeiro, Brazil

ABSTRACT

Oil well drilling demands rapid geological interpretation and timely decision-making, often under complex subsurface conditions. While conventional tools such as drilling parameters, gas analysis, well logs, and cuttings descriptions provide valuable information, additional analytical techniques are often required for greater stratigraphic resolution and accuracy. This study demonstrates the integration of X-ray fluorescence (XRF) and X-ray diffraction (XRD) analyses of drilling cuttings at the wellsite, applied to characterize the Pre-Alagoas Unconformity. This boundary marks the transition between the Itapema and Barra Velha formations in the Brazilian Pre-Salt. Data from 19 wells reveal that, in intervals with minimal barite contamination and limited silicification or dolomitization, XRF successfully identifies variations in the Ca/Sr ratio across the unconformity. The Barra Velha Formation exhibits lower Ca/Sr ratios and higher Sr contents than the Itapema Formation, indicating elevated paleosalinity and distinct carbonate precipitation dynamics. XRD provides mineralogical validation, while statistical filtering and non-parametric testing confirm that these geochemical contrasts are significant and robust. These findings establish the Ca/Sr ratio as a reliable stratigraphic discriminator in lacustrine carbonate successions and highlight the practical value of combining XRF, XRD, and statistical methods for enhanced real-time geological interpretation during drilling operations.

Keywords: Pre-Salt, Santos Basin, Barra Velha Formation, Itapema Formation, geochemical stratigraphy.

RESUMO

A perfuração de poços de petróleo exige interpretação geológica rápida e tomada de decisão assertiva, frequentemente sob condições subsuperficiais complexas. Embora ferramentas convencionais, como parâmetros de perfuração, análise de gases, perfis de poço e descrição de amostras de calha, forneçam informações essenciais, técnicas analíticas adicionais são frequentemente necessárias para maior resolução e precisão estratigráfica. Este estudo demonstra a integração das análises de fluorescência de raios-X (XRF) e difração de raios-X (XRD) de amostras de calha no local da perfuração para caracterizar a Discordância Pré-Alagoas, que marca o limite entre as formações Itapema e Barra Velha no Pré-Sal brasileiro. Dados de 19 poços revelam que, em intervalos com mínima contaminação por barita e limitada silicificação ou dolomitização, a XRF identifica com sucesso variações na razão Ca-Sr ao longo da discordância. A Formação Barra Velha apresenta razões Ca-Sr mais baixas e teores de Sr mais elevados do que a Formação Itapema, indicando maior paleossalinidade e dinâmicas distintas de precipitação carbonática. A XRD fornece validação mineralógica, enquanto a filtragem estatística e os testes não paramétricos confirmam que esses contrastes geoquímicos são significativos e robustos. Esses resultados estabelecem a razão Ca-Sr como um discriminador estratigráfico confiável em sucessões carbonáticas lacustres e destacam o valor da combinação entre XRF, XRD e métodos estatísticos para aprimorar a interpretação geológica em tempo real durante operações de perfuração.

Palavras-chave: Pré-sal, Bacia de Santos, Formação Barra Velha, Formação Itapema, estratigrafia geoquímica.

Recebido: 15 de maio de 2025 | Recebido no formato de revisão: 05 de agosto de 2025 | Aceito: 04 de setembro de 2025 | Disponível online: 27 de outubro de 2025

DOI: https://doi.org/10.70369/6rnx5120

1. INTRODUCTION

During oil well drilling operations, numerous geological interpretations and operational decisions must be made rapidly to ensure both process efficiency and drilling safety (Oliveira et al., 2022a; 2022b; 2024). To support these decisions, several real-time monitoring tools are employed, including drilling parameters (e.g., rate of penetration, torque, RPM, and weight on bit), formation gas analysis (methane, ethane, propane, butane, and pentane), cuttings descriptions, and Logging While Drilling (LWD) logs. Collectively, these tools facilitate real-time geological interpretation and the identification of fluids and stratigraphy (Ellis and Singer, 2008; Craigie, 2018; Oliveira et al., 2022b; Gonzaga et al., 2024; Leon et al., 2024).

In geologically complex scenarios, such as intervals containing volcanic rocks or during the drilling of reservoir sections, cuttings samples are frequently subjected to additional analytical techniques, including X-ray fluorescence (XRF) and X-ray diffraction (XRD). These methods provide chemical and mineralogical characterization, respectively, of cuttings collected at standard three-meter intervals (Oliveira et al., 2022a).

Accordingly, the objective of this study is to characterize the Pre-Alagoas Unconformity (DPA), which marks the boundary between the Itapema and Barra Velha formations, through integrated XRF and XRD analyses of cuttings samples acquired during drilling operations.

1.1. Geological context of the Pre-Salt interval in the Santos Basin

The Pre-Salt interval of the Santos Basin (Figure 1) presents a complex geological framework (Penna et al., 2019), comprising three main formations: Barra Velha, Itapema, and Piçarras (Moreira et al., 2007; Araújo et al., 2024).

The Barra Velha Formation consists of carbonates deposited in alkaline lacustrine environments (Pietzsch et al., 2020; Herlinger Jr. et al., 2020), featuring structures such as spherulites, shrubs, and magnesium-rich clay minerals (Gomes et al., 2020). These carbonates are often affected by dolomitization or silicification, processes that significantly modify their original porosity (Wright and Barnett, 2020; Herlinger Jr. et al., 2020; Satorato et al., 2020).

The Itapema Formation comprises carbonates composed of dolomitized or silicified bivalve shells and organic-rich dark shales, both deposited in lacustrine settings (Moreira et al., 2007; Chinelatto et al., 2020).

The Piçarras Formation includes sandstones, pelites, and hybrid rocks, with occurrences of "talc-stevensite" (a classical designation for magnesium-rich clay fragments) in lacustrine deposits and alluvial fan deposits in proximal areas (Moreira et al., 2007; Leite et al., 2020; Amorim et al., 2024).

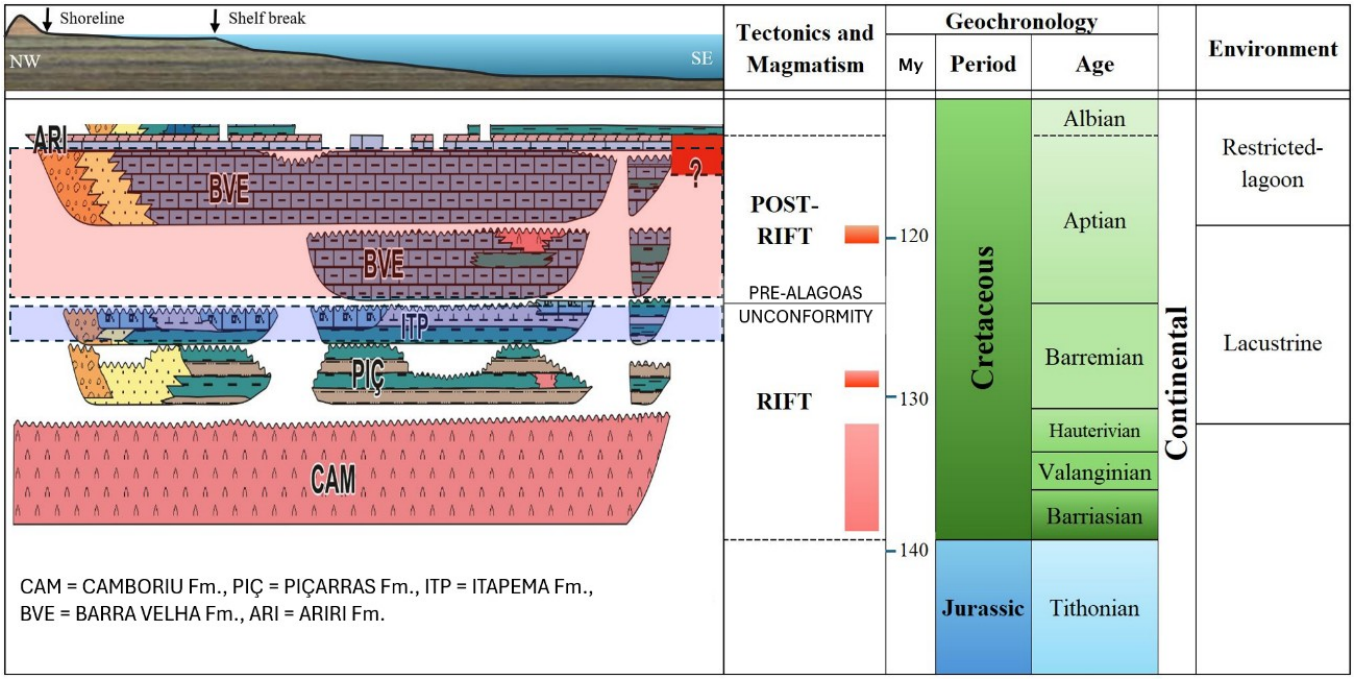

Figure 1. Stratigraphic Chart of the Santos Basin highlighting the Pre-Salt section, represented by the Camboriu, Piçarras, Itapema (highlighted in blue), and Barra Velha (highlighted in red) formations. The contact between the Itapema and Barra Velha formations corresponds to the Pre-Alagoas Unconformity.

The contact between the Piçarras and Itapema formations is readly recognized due to diagnostic features in density, neutron, sonic, resistivity, and nuclear magnetic resonance logs, primarily influenced by the elevated magnesium clay content in the older unit (Amorim et al., 2024). However, the absence of distinctive log responses at the boundary between the Itapema and Barra Velha formations poses challenges for real-time identification of the Pre-Alagoas Unconformity. Although the presence of coquinas in cuttings samples would typically indicate the Itapema Formation, their recognition is often hindered by the fragmentation process during drilling. Reliable identification is possible only when well-developed coquina zones are encountered or when Jiquiá source rocks occur at the top of the unit, producing characteristic well log responses.

1.2. Geological operations and cuttings sampling during well drilling

Geological Operations comprise a field of applied geoscience in which geological interpretation is performed in real time during drilling, using tools and equipment available on the rig in both onshore and offshore environments. The primary tools employed include Logging While Drilling (LWD) systems, mudlogging equipment (for gas analysis, drilling parameters, and calcimetry), complementary geochemical and mineralogical techniques (XRF and XRD), and descriptions of cuttings samples retrieved during drilling.

Cuttings are rock fragments generated by the drill bit during wellbore advancement. These fragments are transported to the surface by the drilling fluid, and their corresponding depths are calculated using a mathematical approach known as lag time (Bourgoyne Jr. et al., 1986), which accounts for the fluid's travel time from the bit to the surface. Typically, cuttings are assigned to the depth corresponding to the base of the three-meter interval they represent. However, these samples are often accompanied by non-formation materials, such as drilling fluid solids (e.g., crystalline calcite and barite) and iron filings derived from the bit, casing, or drill string.

1.3. Application of XRF and XRD analyses in real-time lithological characterization

X-ray fluorescence (XRF) and X-ray diffraction (XRD) analyses are applied to determine the chemical composition and mineralogy of cuttings samples, supporting real-time lithological characterization (Oliveira et al., 2022b). This approach leverages cuttings, which are collected from all drilled wells and are generally representative of nearly all stratigraphic units (Craigie, 2018). Samples are collected cumulatively at three-meter intervals and referenced to the depth corresponding to the base of each interval.

During drilling, compact equipment must be used. These typically offer lower precision than laboratory instruments. Sophisticated WDXRF (Wavelength Dispersive X-ray Fluorescence) instruments cannot be used on drilling rigs due to harsh operating conditions. Despite their superior resolution and detection limits compared to EDXRF (Energy Dispersive X-ray Fluorescence), they are replaced by EDXRF devices, which are more compact and robust for rig-site applications (Kaur and Singh, 2024).

To address these operational limitations and ensure data reliability, several quality control procedures were implemented. Daily calibration checks were performed using internationally certified basalt, carbonate, and siliciclastic rock standards, analyzed every 12 hours, to monitor potential instrument drift. Duplicate analyses were carried out every ten samples to assess repeatability, and cross-validation between XRF and XRD results was performed to improve mineralogical interpretation. Additionally, consistency between major and trace element trends was regularly assessed to detect anomalous readings and improve data reliability. Although specific detection limits and factory calibration curves provided by service companies were unavailable, these procedures allowed for continuous verification of analytical consistency in the field (Pessanha et al., 2009; Craigie, 2018; Oliveira et al., 2022b).

Contamination by drilling fluids typically occurs through impregnation by oil-based or water-based fluids, often containing barite-based viscosifiers (Craigie, 2018; Abdou et al., 2018). Prior to XRF and XRD analysis, cuttings samples undergo cleaning to reduce fluid contamination, as described by Oliveira et al. (2022b). Barite contamination is quantified using an established equation, and samples exceeding 10% contamination are discarded (Oliveira et al., 2022b). Cross-validation with XRD results is also necessary to monitor barite content.

Analyses are conducted onboard the drilling rig within a few hours of the samples being cut by the bit. Data are then stacked according to collection depth. The presence of mixed lithologies within each three-meter interval results in data smoothing, facilitating the recognition of chemofacies boundaries and enabling modeling at the scale of stratigraphic units. This also supports the identification of regional geochemical and mineralogical variations, formation boundaries, unconformities, and changes in sediment provenance (Craigie, 2018; Ribeiro, 2019; Saibro, 2021; Ribeiro, 2021; Ramos, 2022; Imbuzeiro, 2021; Oliveira et al., 2022b; Rocha, 2024; Imbuzeiro et al., 2024).

For Geological Operations, these tools are essential for identifying volcanic sections and associated intrusions, characterizing silicification and dolomitization zones in Pre-Salt carbonates, and supporting stratigraphic positioning during drilling by delineating formation changes and unconformities (Oliveira et al., 2022b).

1.4. Sr/Ca ratios in calcite as a proxy for lacustrine carbonate systems

The Sr/Ca ratio in calcite has been widely explored as a geochemical proxy for reconstructing paleoenvironmental conditions (Gagan et al., 1998, Langer et al., 2006, Tang et al., 2008a, Tang et al., 2008b). Experimental studies demonstrate that Sr incorporation into the calcite lattice is primarily controlled by precipitation kinetics, with higher growth rates leading to greater Sr partitioning (Tang et al., 2012). While ionic strength (a proxy for salinity) exerts a secondary influence, its effect on Sr incorporation is comparatively minor relative to precipitation rate (Tang et al., 2012).

However, studies on natural lacustrine systems, such as the Black Sea, reveal that changes in water chemistry, particularly salinity shifts, can also significantly affect Sr/Ca ratios at a basin scale (Bahr et al., 2008). This implies that variations in Sr/Ca ratios may reflect a combination of water chemistry and calcite growth dynamics, offering insights into salinity and saturation conditions during carbonate deposition.

In the context of the Pre-Salt carbonates of the Santos Basin, where Barra Velha and Itapema formations were formed under distinct lacustrine chemistries, Sr/Ca ratios provide a valuable tool for differentiating depositional environments and enhancing the identification of the Pre-Alagoas Unconformity.

2. MATERIALS AND METHODS

This study is based on cuttings descriptions and XRF and XRD analyses from 19 wells in the Santos Basin (Table 1). Cuttings descriptions, initially performed in real time during drilling operations, were subsequently revisited and selectively reinterpreted post-drilling. Sampling was carried out at regular three-meter intervals, with depths referenced to the base of each interval.

XRF and XRD data were acquired on the rig using the cuttings samples collected during drilling. Analyses followed the bulk method, in which the entire sample volume was ground and analyzed without prior lithological separation. Due to operational constraints during drilling, not all samples were analyzed; instead, one out of every three samples was selected for processing. This sampling followed a standardized interval-based approach, with no lithological or geochemical selection criteria applied, ensuring systematic coverage of the drilled sections.

Prior to analysis, samples were washed with a neutral detergent to minimize drilling fluid influence, oven-dried at 80 °C, and ground using an agate mortar until all particles passed through a 150 µm sieve. Subsequently, magnetic separation was performed to remove metallic fragments derived from the drill bit or casing (Figure 2).

XRF analyses were conducted using the following instruments (Table 1): Delta Premium Handheld (Pd filament; 10 min), Xepos Standard (Pd filament; 10 min), Panalytical Epsilon 1 (Ag filament; 10 min), Spectro Xepos O3STD Vacuum/Ametek (Pd filament; 10 min), and Bruker S2 Puma (Pd filament; 10 min). Depending on the instrument, samples were prepared using either the loose powder method with a sample cup (Delta Premium Handheld and Panalytical Epsilon 1) or pelletized (Xepos Standard, Spectro Xepos O3STD Vacuum/Ametek, and Bruker S2 Puma).

The following major and minor elements were quantified in weight percent (%): Na, Mg, Al, Si, P, S, K, Ca, Ti, Mn, and Fe; and trace elements in parts per million (ppm): Cl, V, Cr, Co, Ni, Cu, Zn, Ga, Ge, As, Se, Br, Rb, Sr, Y, Zr, Nb, Mo, Ag, Cd, Sn, Sb, Te, I, Cs, Ba, La, Ce, Hf, Ta, W, Hg, Tl, Pb, Bi, Th, and U.

To ensure data reliability, a rigorous field validation protocol was implemented, combining multiple quality control procedures. These included: (1) duplicate analyses every ten samples to assess repeatability (figures 3A, 3B); (2) analysis of internationally certified rock standards: carbonates (SRM88B, 1D, SR1), basalt (USGS BCR-2), and siliciclastic materials, every 12 hours to monitor instrument stability and drift (Figure 3C); (3) comparison of major and trace element trends within the XRF dataset to identify anomalous readings; and (4) cross-validation of XRF results with XRD mineralogical data from the same samples. These standards encompass a broad range of Ca and Sr concentrations, providing reliable reference points for the key elements of interest in this study.

Although factory-provided detection limits and calibration curves were unavailable from the service companies, these procedures ensured qualitative to semi-quantitative control of analytical performance, effectively mitigating uncertainties inherent to rig-based XRF analyses. Barite contamination was monitored and quantified following the method described by Oliveira et al. (2022b).

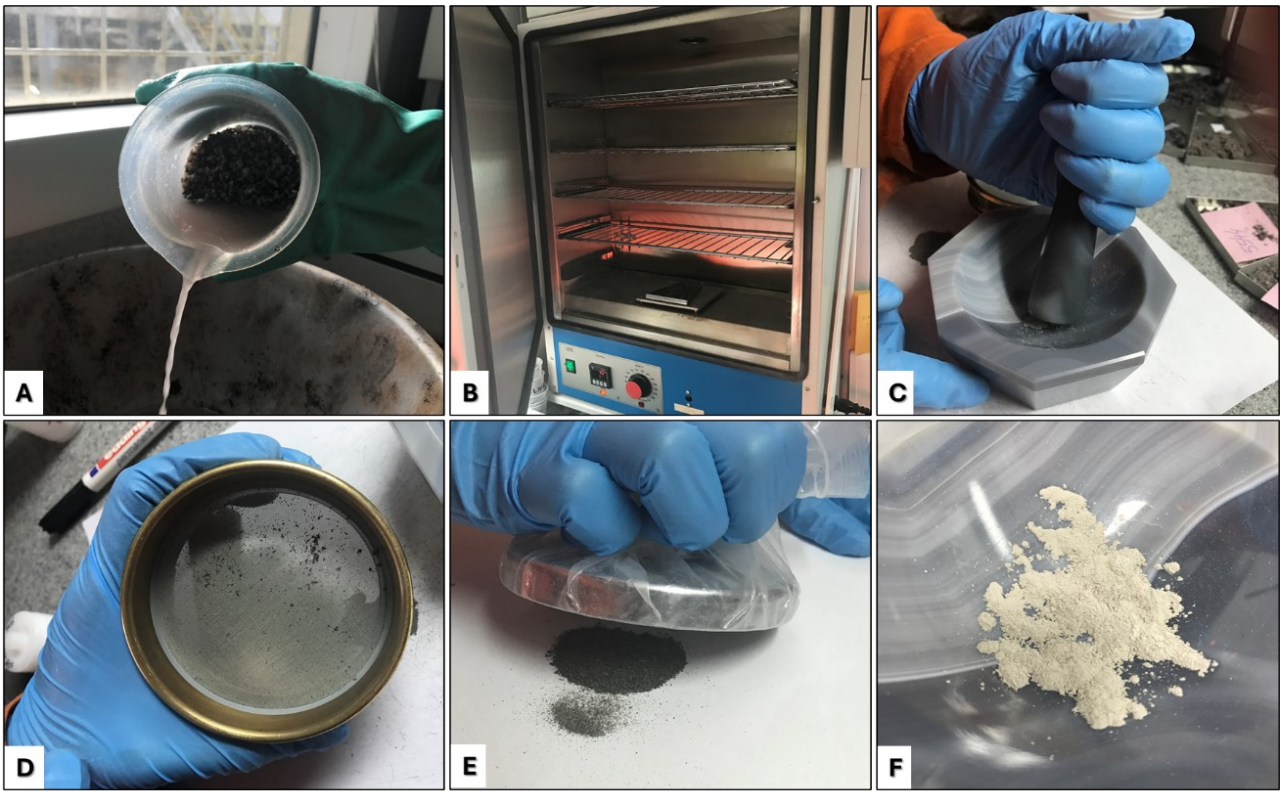

Figure 2. Sample preparation steps conducted on the drilling rig. **A.** Washing with neutral detergent to remove excess drilling fluid. **B.** Drying in an oven at 80 °C. **C.** Grinding using an agate mortar. **D.** Sieving through a 150 µm mesh (coarser fractions were reground until the entire sample passed through). **E.** Magnetic separation to remove metallic fragments from the bit or casing. **F.** Prepared sample ready for analysis.

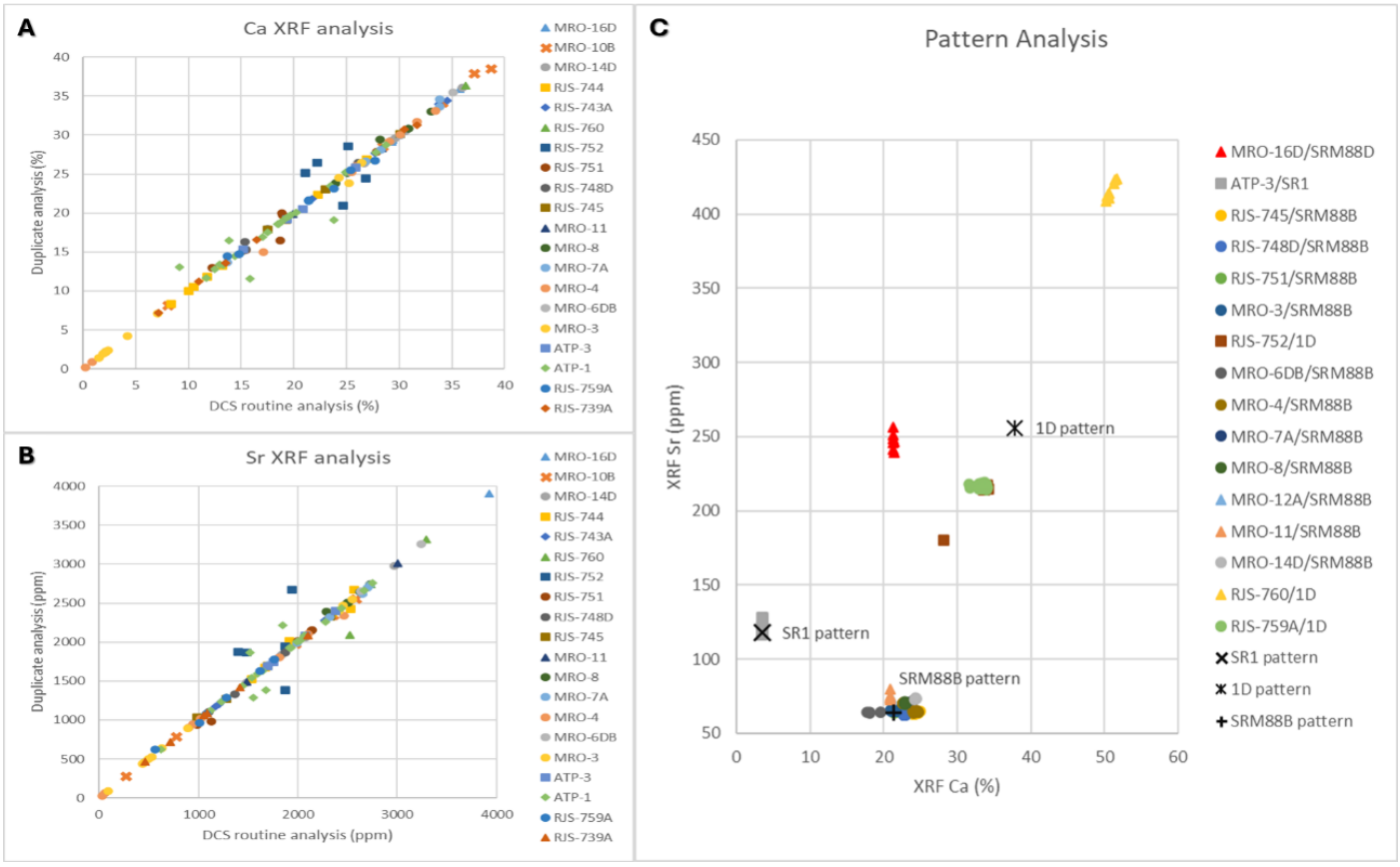

Figure 3. Quality control procedures. **A-B.** Correlation between duplicate analyses of Ca and Sr performed every ten samples. **C.** Ca vs. Sr plot comparing three carbonate standards (SRM88B, 1D, and SR1), illustrating qualitative to semi-quantitative analytical consistency.

Although major elements in geochemical datasets are typically reported as oxides, this study presents them in elemental form. This approach reflects standard practices in geological operations, where oxide-to-element conversions are routinely applied to facilitate comparison with lithogeochemical logs, despite being non-standard in academic reporting.

For XRD analyses, the following instruments were used (Table 1): X Benchtop (CoKα1; 30 min; 0.3 mA; 30 kV), Olympus (CoKα1; 30 min; 0.3 mA; 30 kV), and Bruker D2 Phaser (CuKα1; 16 min; 10 mA; 30 kV). Samples were prepared and analyzed on the rig, and diffractograms were subsequently reinterpreted using Bruker DIFFRAC.EVA software. Mineral percentages were estimated using the Reference Intensity Ratio (RIR) method (Hubbard and Snyder, 1988), consistent with procedures applied during drilling operations.

Descriptive statistics for Ca, Sr, and Ca/Sr were calculated for each formation, including mean, median, standard deviation, minimum, maximum, and 95% confidence intervals. To evaluate differences between formations, Mann–Whitney U and Kruskal–Wallis non-parametric tests were applied. Effect size (Cohen's d) was computed to quantify the magnitude of these differences.

An outlier filtering approach was implemented to exclude samples with anomalously high Ba (barite contamination) and Si (related to silicification). Pearson and Spearman correlation coefficients were calculated before and after filtering to assess the impact of contamination and diagenetic overprints on the Ca–Sr relationship.

3. RESULTS

In the 19 wells analyzed, cuttings descriptions were compared with XRD and XRF results, as detailed in the following sections. Table 1 lists the 12 wells where a distinct feature could be identified between the Ca and Sr curves derived from XRF analyses.

3.1. Lithological description of cuttings

Based on cuttings descriptions obtained during drilling, three lithological types were identified: (1) undifferentiated limestone, (2) coquina, and (3) laminite (Figure 4).

Table 1. List of wells with XRD and XRF analyses (indicating whether sampling was sequential at 9 m intervals or performed at specific points) and identification of the presence or absence of the Ca–Sr trend in the XRF data, including observations related to mineralogy or barite contamination. Abbreviations for XRF and XRD instruments: XS – EDXRF Xepos Standard; DPH – EDXRF Delta Premium Handheld; PE – EDXRF Panalytical Epsilon 1; S2 – EDXRF Bruker S2 Puma; SX – EDXRF Spectro Xepos O3STD Vacuum/Ametek; XB – XRD X Benchtop; OL – XRD Olympus; D2 – Bruker D2 Phaser.

Wells	XRF	XRF instrument	XRD	XRD instrument	Ca-Sr feature	Observations
3-RJS-739A	9x9m	XS	Punctual	XB	present	
9-ATP-1-RJS	9x9m	XS	9x9m	XB	absent	Baritine contamination
9-ATP-3-RJS	9x9m	DPH	9x9m	XB	absent	High silicification
3-RJS-743A	9x9m	XS	9x9m	XB	absent	High dolomitization
3-RJS-744	9x9m	DPH	9x9m	XB	absent	Baritine contamination
3-RJS-745	9x9m	DPH	9x9m	OL	present	Low to moderate silicification
3-RJS-748D	9x9m	SX	9x9m	D2	absent	Baritine contamination
3-RJS-751D	9x9m	SX	9x9m	D2	absent	Jiquia source rock present
7-MRO-3-RJS	9x9m	SX	9x9m	D2	present	Low to moderate dolomitization
1-RJS-752	9x9m	PDH	9x9m	D2	present	
7-MRO-6DB-RJS	9x9m	SX	9x9m	OL	present	
8-MRO-4-RJS	9x9m	SX	9x9m	D2	present	
7-MRO-7A-RJS	9x9m	SX	9x9m	D2	present	
7-MRO-10B-RJS	9x9m	PE	9x9m	OL	present	
8-MRO-8-RJS	9x9m	SX	9x9m	D2	present	
8-MRO-12A-RJS	9x9m	S2	9x9m	D2	absent	Silicification and dolomitization presents
8-MRO-11-RJS	9x9m	S2	9x9m	D2	present	
8-MRO-14D-RJS	9x9m	SX	9x9m	D2	present	
7-MRO-16D-RJS	9x9m	S2	9x9m	D2	present	

The various limestone types (figures 4A, 4B, 4C, 4I) were grouped as undifferentiated limestones, as the small size of cuttings fragments precludes observation of larger-scale structures. The carbonate facies of the Barra Velha Formation and reworked limestones of the Itapema Formation are typically white, light brown, or dark brown when impregnated with hydrocarbons. When dolomitized (figures 4C, 4D), these rocks acquire a brown color and saccharoidal luster. Intensely silicified lithologies (figures 4E, 4F) appear whitish or translucent, resembling quartz veins.

Bioclastic rudstones (Figure 4H), also referred to as coquinas, are predominantly composed of disarticulated, broken, and amalgamated bivalve shell fragments. Their occurrence is characteristic of the Itapema Formation, although their recognition in cuttings is challenging due to fragmentation during drilling.

Laminites (Figure 4B) consist of thinly interbedded carbonate and siliciclastic or clay layers. In cuttings, these rocks exhibit darker colors, ranging from light brown to black. Along with dark-gray shales (Figure 4G), they are characteristic of Jiquiá-level deposits within the Itapema Formation but may also occur in magnesium clay-rich intervals of the Barra Velha Formation.

3.2. XRF data and variation of key elements

XRF data can be processed and interpreted in various ways. However, for this study, the focus was on variations in calcium (Ca), silicon (Si), magnesium (Mg), iron (Fe), aluminum (Al), potassium (K), barium (Ba), strontium (Sr), zirconium (Zr), and rubidium (Rb).

In 12 of the 19 wells, a clear variation in Sr behavior relative to Ca was observed across the Pre-Alagoas Unconformity (Table 1). Within the Barra Velha Formation, Sr values are consistently higher than in the Itapema Formation for equivalent Ca contents when considering only carbonate rocks (Figure 5). In some wells, this contact is additionally marked by the presence of Jiquiá-age laminites, which are characterized by elevated Al, Fe, Si, K, Rb, and Zr contents (Figure 6). In contrast, laminites within the Barra Velha Formation exhibit increases primarily in Al, Fe, and Mg. In the remaining seven wells, increased Si, Mg, Fe, or Ba, occurring either independently or in combination, obscured the trend, resulting in the absence of the Ca–Sr pattern (Figure 7).

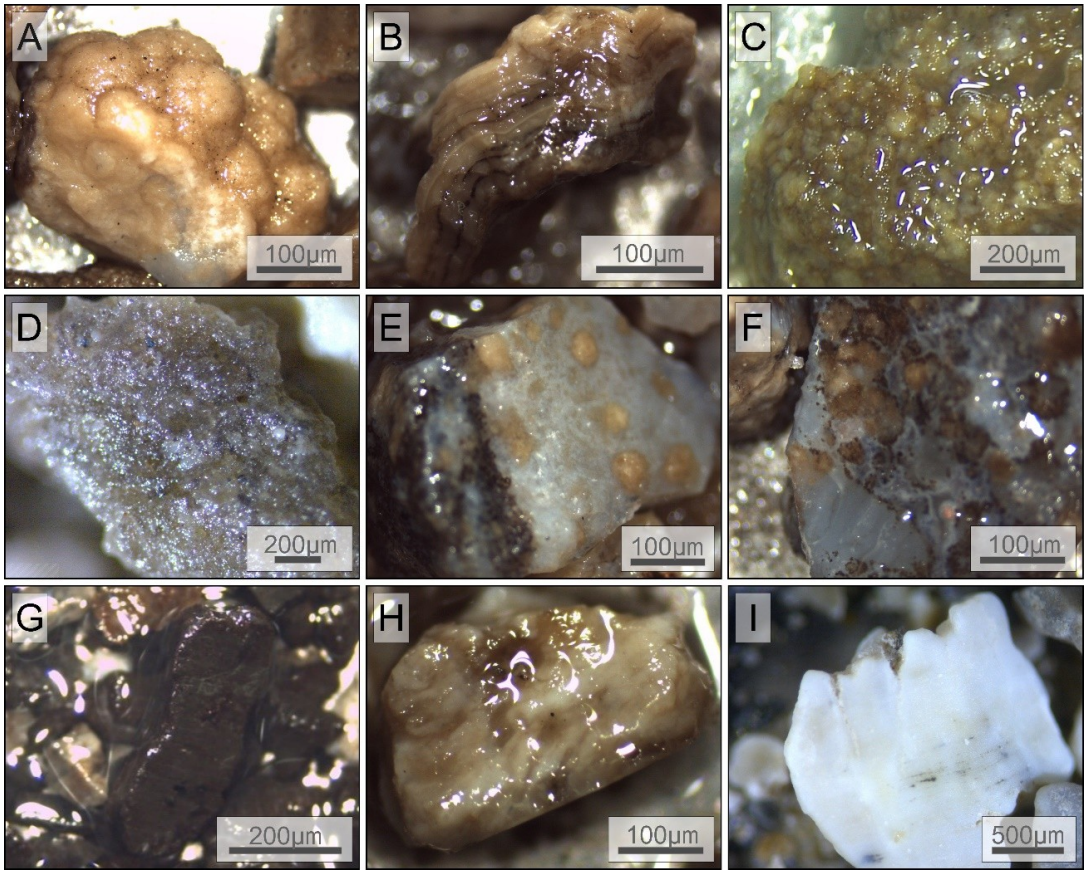

Figure 4. Cutting samples of the main lithologies encountered during drilling in the Pre-Salt succession of the Santos Basin. **A.** Partially silicified shrubstone. **B.** Laminite. **C.** Partially dolomitized spherulitic carbonate (spherulstone). **D.** Microcrystalline dolomite. **E.** Intensely silicified spherulitic carbonate (spherulstone). **F.** Intensely silicified shrubstone. **G.** Dark gray "Jiquiá" shale. **H.** Bioclastic rudstone (coquina) with disarticulated fragments. **I.** Mudstone.

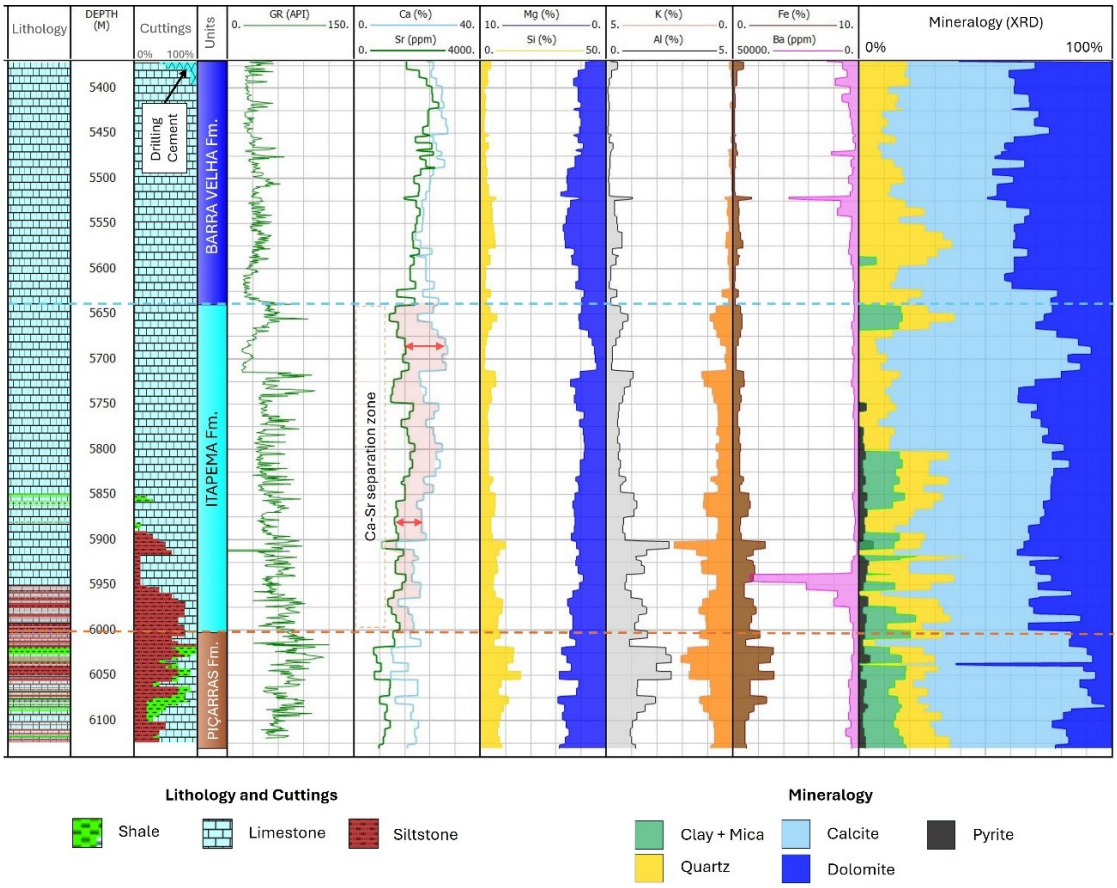

Figure 5. Well 1-RJS-752 showing the Ca–Sr trend at the Pre-Alagoas Unconformity, marking the contact between the Itapema and Barra Velha formations.

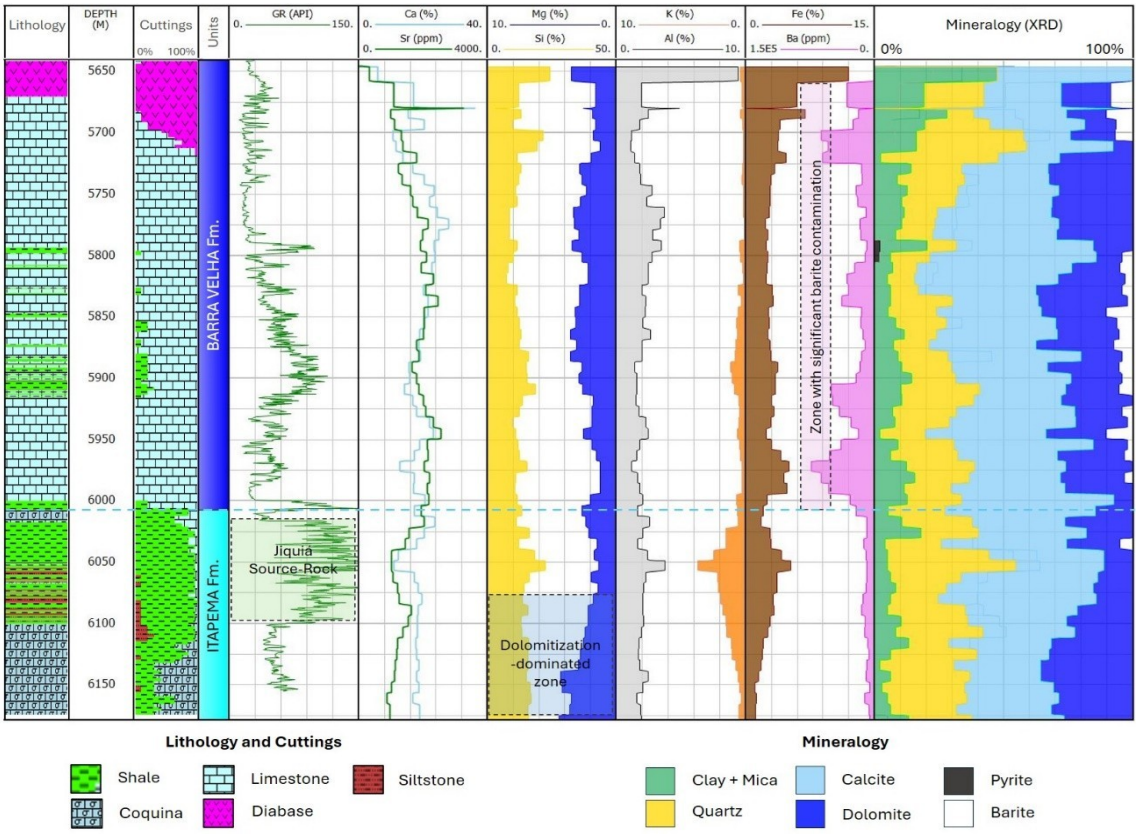

Figure 6. Well 3-RJS-751 showing the Jiquiá source rock at the top of the Itapema Formation, with elevated K values. The well also shows evidence of barite contamination in the Barra Velha section (high Fe and Ba in XRF, and clay+mica in XRD) and intense dolomitization in the Itapema coquina interval.

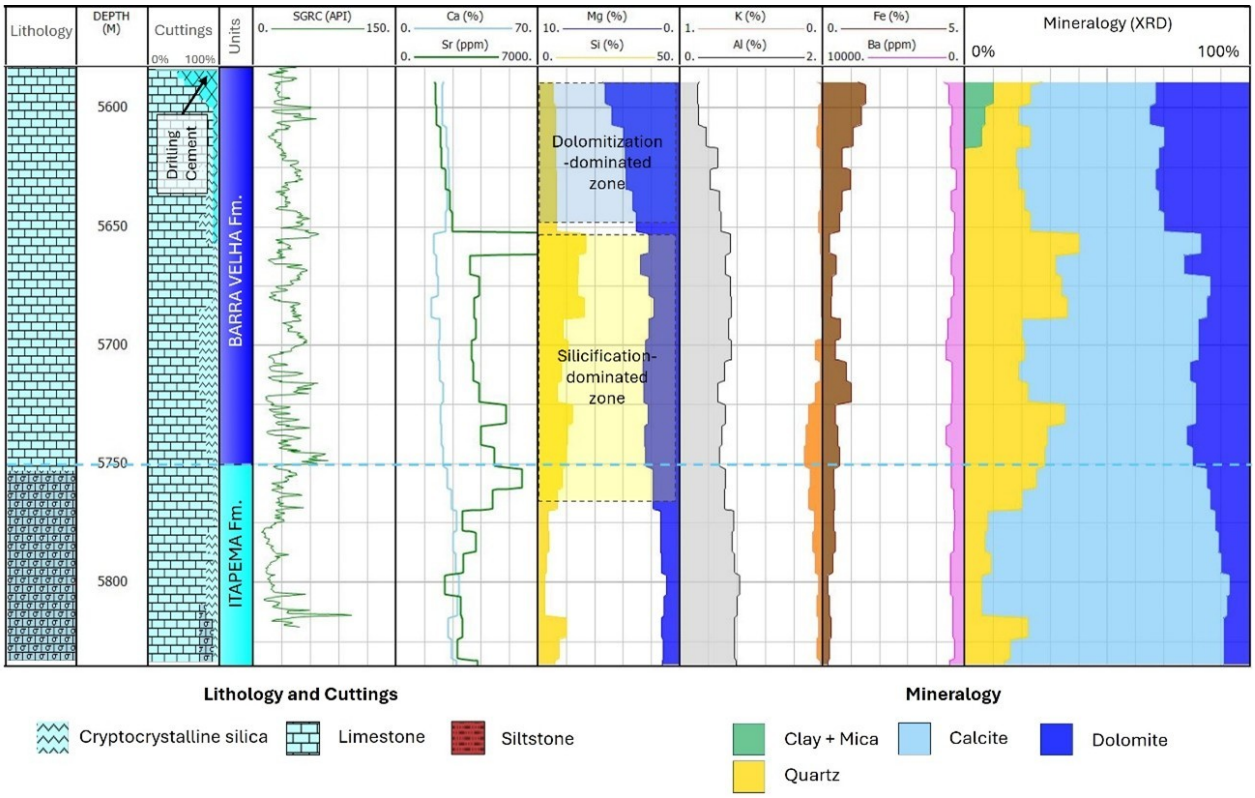

Figure 7. Well 8-MRO-12A-RJS showing the absence of the Ca–Sr trend due to high silicification in the cuttings, evidenced by quartz in XRD and elevated Si values when Al and Fe are below 1%. In highly dolomitized intervals, the trend also deviates from typical Barra Velha Formation behavior.

3.3. X-Ray diffraction analysis and mineralogical variations

XRD confirmed the mineralogical variations inferred from XRF. Carbonate rocks of the Barra Velha and Itapema formations are predominantly composed of calcite, dolomite, and quartz. In Jiquiá-level laminites of the Itapema Formation, clays or mica (characterized by the 10 Å reflection), feldspars (primarily potassium feldspar with minor plagioclase), and quartz are present (Figure 8).

These relationships are visualized in Figure 9, where regression analyses with 95% confidence intervals are shown for original and outlier-removed datasets. Non-parametric statistical testing confirms that Ca/Sr differs significantly between formations (Mann–Whitney U, $p < 0.001$; Kruskal–Wallis $H = 42.41$, $p < 0.001$), with a moderate effect size (Cohen's $d = -0.398$). These findings support the use of this ratio as a discriminant between formations.

The presence of quartz in carbonates correlates with elevated Si. Similarly, increased dolomite content correlates with higher Mg when unaccompanied by Fe and Al increases. When Si and Mg increases coincide with elevated Fe and Al, XRD indicates the presence of clay minerals. Barite peaks in diffractograms are commonly associated with elevated Ba and Fe in XRF data.

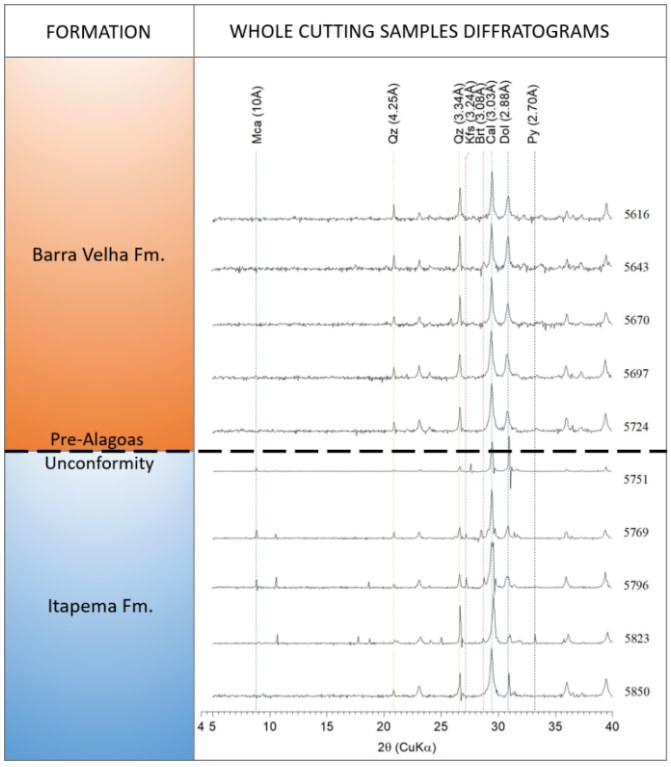

Figure 8. X-Ray diffractograms of well 7-MRO-16D-RJS used for mineralogical control during drilling, showing that the carbonate rocks of the Barra Velha and Itapema formations are predominantly composed of calcite, dolomite, and quartz.

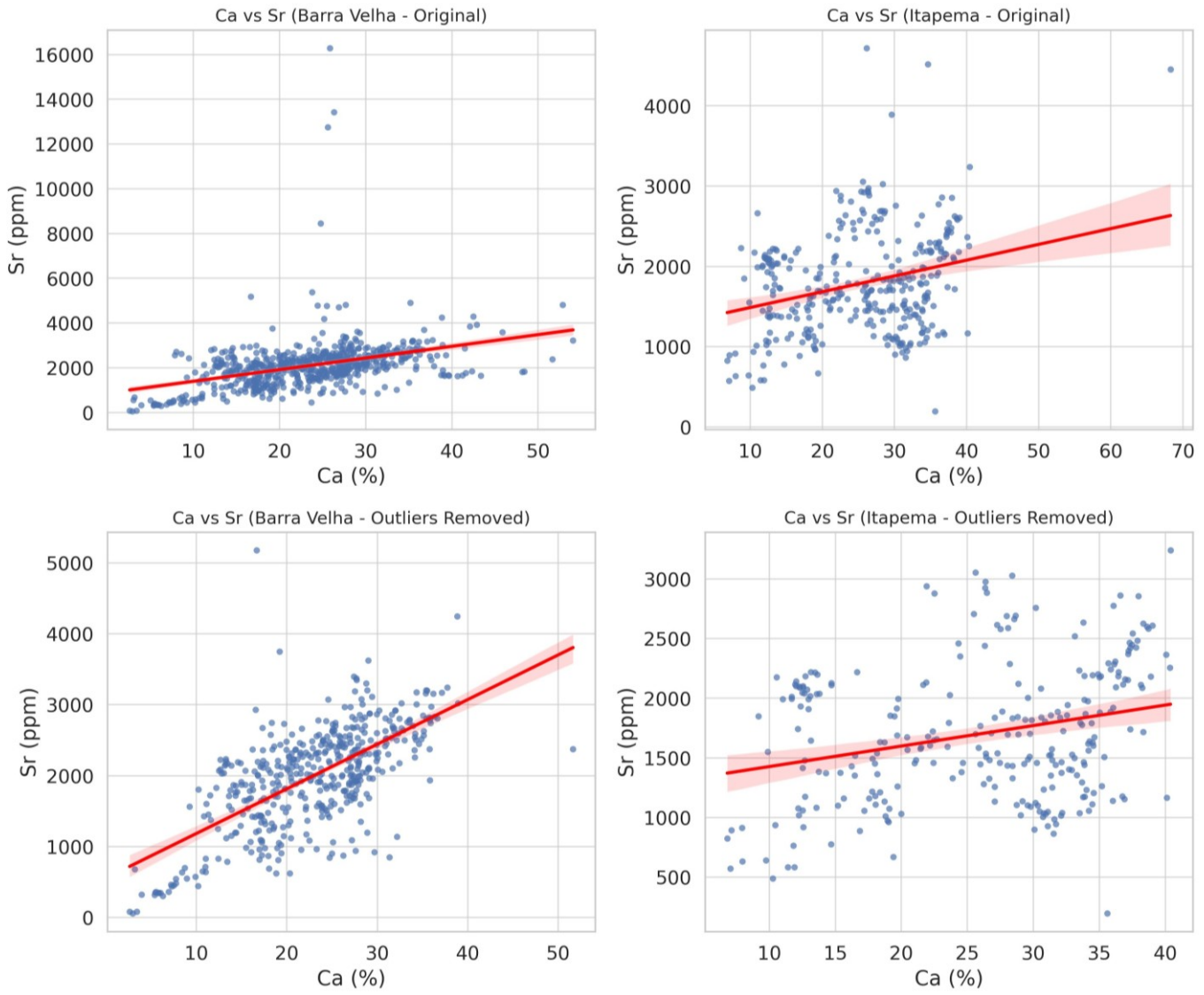

Figure 9. Regression analyses for Ca vs. Sr with 95% confidence intervals, shown for both original and outlier-removed datasets.

3.4. Statistical assessment of Ca, Sr, and Ca-Sr variability between formations

Descriptive statistics for Ca, Sr, and Ca-Sr in the Barra Velha and Itapema formations are presented in Table 2. On average, the Barra Velha Fm. shows slightly lower Ca concentrations and higher Sr contents than the Itapema Fm., resulting in lower Ca-Sr ratios.

The mean Ca content in Barra Velha Fm. is 23.45% (95% CI: 22.82–24.07%), while in Itapema Fm. it reaches 25.26% (95% CI: 24.30–26.22%). Sr concentrations average 2095.13 ppm in Barra Velha Fm. (95% CI: 2006.90–2183.36 ppm) and 1787.38 ppm in Itapema Fm. (95% CI: 1720.08–1854.67 ppm). Ca-Sr ratios average 0.0127 in Barra Velha Fm. (95% CI: 0.0122–0.0131) and 0.0158 in Itapema Fm. (95% CI: 0.0146–0.0170).

These differences are illustrated in Figure 10, which displays boxplots for Ca, Sr, and Ca-Sr, highlighting their distinct distributions across formations. Ba and Si contents, which can indicate barite contamination and silicification, are summarized in Table 3. Barra Velha Fm. shows higher mean Ba (≈41,951 ppm) and Si (≈9.38%) than Itapema Fm., with considerable variability (Table 3).

Correlation coefficients for Ca and Sr are presented in Table 4. In Barra Velha Fm., the Pearson correlation increases from 0.370 (all samples) to 0.655 after outlier removal, showing a substantial improvement when high Ba and Si samples are excluded. For Itapema Fm., the correlation remains relatively stable, with Pearson coefficients of 0.281 (all samples) and 0.272 (outlier-removed).

Table 2. Descriptive statistics for Ca, Sr, and Ca-Sr in Barra Velha and Itapema formations (mean, median, std, min, max).

Elements	Statistics	Barra Velha Fm.	Itapema Fm.
Ca	Mean	23.448	25.265
Ca	Median	23.915	26.39
Ca	Std	8.193	9.001
Ca	Min	2.61	6.805
Ca	Max	54.05	68.28
Sr	Mean	2095.129	1787.377
Sr	Median	2071.0	1725.0
Sr	Std	1155.239	630.818
Sr	Min	57.0	195.5
Sr	Max	16286.73	4719.0
Ca/Sr	Mean	0.013	0.016
Ca/Sr	Median	0.012	0.015
Ca/Sr	Std	0.005	0.011
Ca/Sr	Min	0.002	0.004
Ca/Sr	Max	0.052	0.182
N		662.0	340.0

Table 3. Descriptive statistics for Ba and Si in Barra Velha and Itapema formations (mean, median, standard deviation, minimum, and maximum values).

Elements	Statistics	Barra Velha	Itapema
Ba	Mean	41951.267	23830.455
Ba	Median	14290.0	5467.0
Ba	Std	86103.97	41384.801
Ba	Min	2.0	2.0
Ba	Max	716900.0	274700.0
Si	Mean	9.385	7.604
Si	Median	7.393	6.48
Si	Std	6.976	5.27
Si	Min	0.054	0.361
Si	Max	47.11	34.55
N		529.0	280.0

Table 4. Pearson and Spearman correlation coefficients for Ca-Sr in the Barra Velha and Itapema formations, calculated with and without outliers.

Correlation Coefficient	Barra Velha (with outliers)	Barra Velha (without outliers)	Itapema (with outliers)	Itapema (without outliers)
Pearson_r	0.37	0.655	0.281	0.272
Spearman_r	0.502	0.63	0.219	0.265
N	661.0	473.0	340.0	272.0

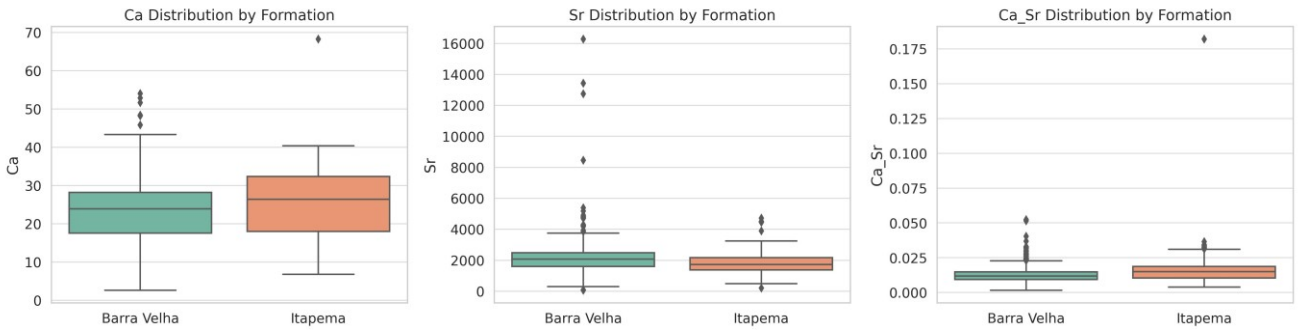

Figure 10. Combined boxplots for Ca (%), Sr (ppm) and Ca-Sr ratio comparing the Barra Velha and Itapema

4. DISCUSSIONS

The chemical and mineralogical correlations derived from XRF and XRD analyses of cuttings provide insights into the origin of the detected chemical elements. These correlations enhance mineralogical control along depth profiles and allow verification of compositional differences between equivalent mineral phases at different depths.

4.1. Differences between Alagoas and Jiquiá carbonates and their paleoenvironmental interpretation

The clear variation in the Ca-Sr ratio observed in XRF analyses of samples from the Barra Velha and Itapema formations reflects the substitution of Sr for Ca within the calcite crystal lattice (Oliveira et al., 2022b). This substitution occurs due to the similarity in ionic radii, oxidation states, and coordination numbers of these elements (Rollinson and Pease, 2021) and serves as a

quality control parameter during drilling operations due to their proportional behavior (Oliveira et al., 2022b).

During calcite precipitation in lacustrine or marine environments, elements such as Mg and Sr are incorporated into the crystal structure depending on their availability in the water (Chivas et al., 1985).

Experimental results from Tang et al. (2015) indicate that Sr incorporation into calcite is primarily driven by precipitation kinetics, whereas the effect of ionic strength (a salinity proxy) is secondary. Conversely, field studies such as Bahr et al. (2008) emphasize that basin-scale variations in Sr/Ca can also record significant salinity changes, particularly in semi-isolated lacustrine systems. Thus, interpreting Sr-Ca variations in the Barra Velha and Itapema formations requires considering both local precipitation dynamics and broader paleo-hydrochemical changes (Chivas et al., 1985; Bahr, 2008).

The observed increase in Sr relative to Ca above the Pre-Alagoas Unconformity in twelve of the wells analyzed (figures 11 and 12) indicates variations in paleosalinity during deposition of the Itapema and Barra Velha formations. Lower salinity conditions during the deposition of the Itapema Formation evolved into higher salinities during deposition of the Barra Velha Formation, corroborating interpretations from other studies (Leite et al., 2020; Netto et al., 2022a; 2022b; Terra et al., 2023; Altenhofen et al., 2024).

4.2. The relationship between dolomitization, silicification, and the Ca-Sr pattern

Dolomitization and silicification are well-documented in the Barra Velha and Itapema formations within the Pre-Salt interval (Basso et al., 2020; Silva et al., 2021; Carvalho et al., 2022; Jesus et al., 2023; Rubim et al., 2024). Dolomitization may be diagenetic, forming small dolomite crystals within fine-grained rocks, or hydrothermal, replacing magnesium-rich clays or calcite (Herlinger et al., 2017; Basso et al., 2020; Carvalho et al., 2022). Silicification in the Barra Velha Formation may result from hydrothermal, depositional, or early diagenetic processes (Herlinger et al., 2017; Basso et al., 2020), whereas in the Itapema Formation, both dolomitization and silicification are often associated with cementation in rudstones (Chinelatto et al., 2020).

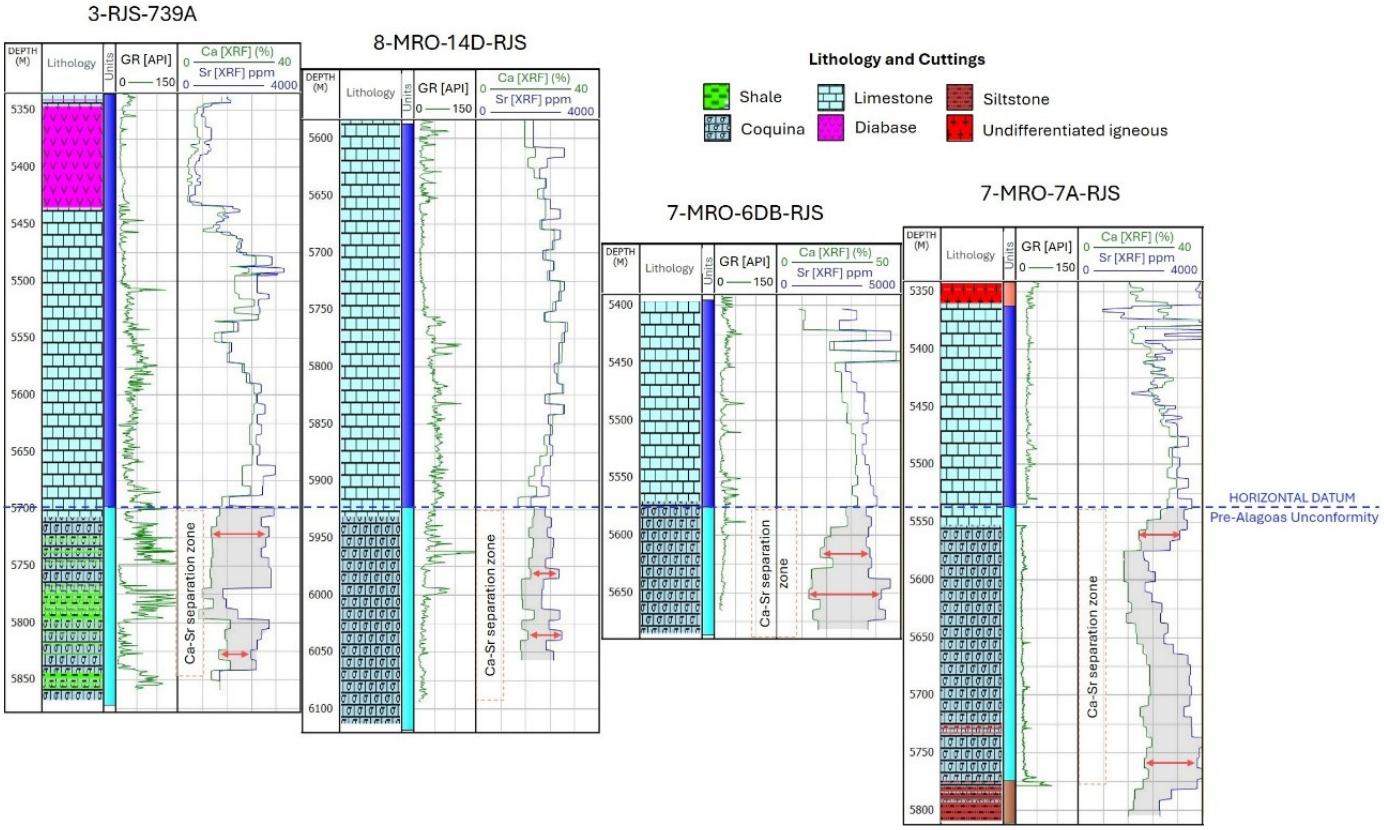

Figure 11. Four of the 12 wells showing the Ca–Sr feature at the discordance between the Barra Velha and Itapema formations in the Mero Field.

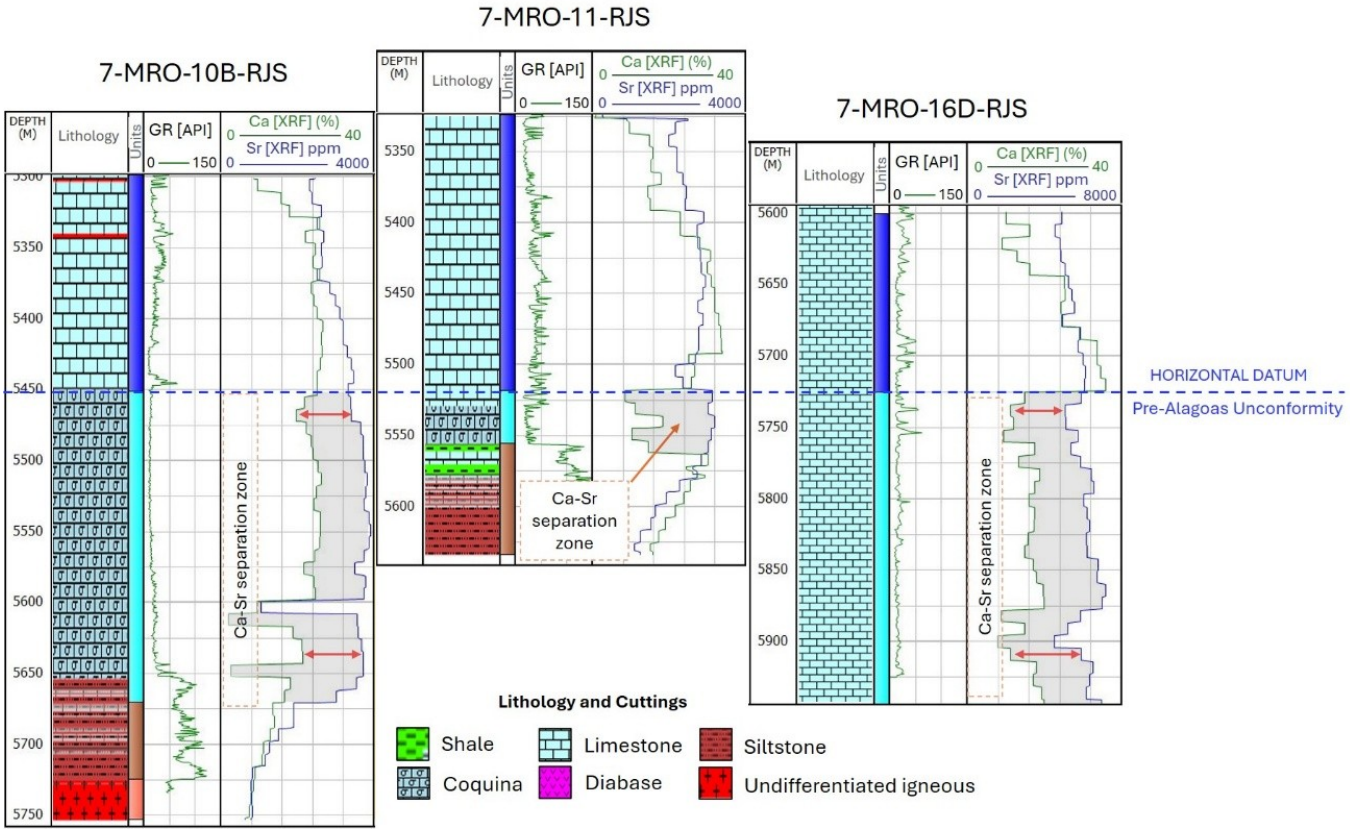

Figure 12. Three of the 12 wells showing the Ca–Sr feature at the discordance between the Barra Velha and Itapema formations in the Mero Field.

Both processes reduce the proportion of calcite in the rock, decreasing the number of crystal lattice sites available for Sr incorporation. Consequently, in wells where these alterations are more intense, the expected Ca–Sr pattern across the Pre-Alagoas Unconformity was not detected, as these diagenetic overprints obscure or even completely mask the original geochemical signal (Figure 7). Additionally, hydrothermal alteration can modify original Sr contents, as Sr is highly mobile in hydrothermal fluids (Yu et al., 2009; Andrews and Jacobson, 2017; Rollinson and Pease, 2021)

4.3. The issue of baritine contamination in cuttings samples

Baritine is a common additive in drilling fluids used to control density and viscosity (Mohamed et al., 2019). Its composition varies by manufacturer but typically includes barite and iron oxides in different proportions (Mohamed et al., 2019; Oliveira et al., 2022b). This material adheres to cuttings and, in some cases, is not fully removed during washing, leading to distortions in XRF results and the appearance of barite and amorphous phases in XRD patterns (Figure 8).

According to Oliveira et al. (2022b), XRF analyses of cuttings with up to 10% barite contamination can still be used. Beyond this threshold, the data are significantly altered, and their use is not recommended. This explains why, in several wells with contamination above this limit, the Ca–Sr pattern was absent or inconsistent, compromising the geochemical interpretation of the Pre-Alagoas boundary.

As the proportion of contaminants increases relative to the rock material, the results become less representative of the actual lithology, particularly for major elements. Trace elements are even more affected due to the presence of iron oxides in the contaminant, since various trace and minor elements can substitute for Fe in these phases (Oliveira et al., 2022b).

Strontium, the key element in the methodology proposed in this study, is highly susceptible to barite contamination because it can substitute for Ba in barite in the same way it substitutes for Ca in calcite (Oliveira et al., 2022b). This results in artificially elevated Sr values, reinforcing the need for rigorous filtering and quality control (Figure 3) to ensure that only minimally contaminated samples are used for interpreting the Ca/Sr ratio.

4.4. Complementarity of XRF and XRD analyses

The integration of XRF and XRD proved fundamental for interpreting the Pre-Alagoas Unconformity, particularly in intervals affected by

diagenetic overprints. In wells where the Ca-Sr pattern was absent, XRF data revealed elevated Si and Mg contents, while XRD corroborated these findings by confirming the presence of quartz and dolomite (Figure 7). Similarly, intervals with increased Ba in XRF analyses were supported by XRD detection of barite, validating contamination from drilling fluids (Figure 6).

These complementary results strengthen the interpretation that the absence of the Ca–Sr trend in specific wells is primarily linked to silicification, dolomitization, or barite contamination rather than analytical inconsistencies. Thus, XRD data not only validate the geochemical signals detected by XRF but also provide mineralogical context, improving the reliability of stratigraphic interpretations across diagenetically altered intervals.

4.5. Statistical assessment of geochemical variability between formations

The geochemical characterization of the Barra Velha and Itapema formations reveals clear and statistically supported differences (tables 2–4). These distinctions enhance the understanding of their depositional and diagenetic histories.

Barra Velha Fm. shows consistently higher Sr contents and lower Ca/Sr ratios than Itapema Fm. (Table 2; Figure 10). This pattern reflects greater Sr incorporation into carbonate phases, likely promoted by elevated paleosalinity and prolonged water–rock interaction during deposition (Bahr et al., 2008, Tang et al., 2012). In contrast, Itapema Fm. exhibits higher Ca contents and elevated Ca/Sr ratios, consistent with less saline conditions and potentially different carbonate precipitation dynamics.

The Mann–Whitney U test ($p < 0.001$) indicates that the distributions of Ca/Sr in these formations differ significantly (Table 4), even without assuming normality. This conclusion is reinforced by the Kruskal–Wallis test ($H = 42.41$, $p < 0.001$), confirming that these differences are not only statistically robust but also geochemically meaningful, reflecting distinct depositional environments.

The marked improvement in Pearson correlation for Barra Velha Fm. after outlier removal (Table 4; Figure 9) underscores the importance of accounting post-depositional alterations. Elevated Ba suggests barite contamination from drilling fluids, while elevated Si suggests episodes of silicification (Table 3; Figure 7). Both processes obscure the primary depositional geochemical signal. By applying targeted filtering to remove these outliers, the underlying Ca–Sr relationship becomes clearer (Figure 9), providing a more reliable representation of the original depositional conditions. This approach improves the interpretability of the dataset and highlights the value of incorporating statistical tools such as outlier detection, effect size measurements, and confidence intervals when using trace elements as stratigraphic proxies.

Collectively, these findings validate the robustness of the Ca/Sr ratio as a stratigraphic discriminator in lacustrine carbonate successions, even in contexts influenced by diagenesis or drilling-related contamination.

4.6. Methodological limitations and implications

The operational context of this study imposes inherent constraints on data acquisition. The use of portable and benchtop XRF instruments onboard drilling rigs, although essential for real-time decision-making, offers lower analytical precision compared to certified laboratory equipment due to limitations in calibration, instrumental stability, and detection limits.

Additionally, barite-based drilling fluids and iron oxide additives contribute to contamination of cuttings samples, potentially altering major and trace element concentrations, especially Sr. These effects are particularly evident in intervals with elevated Ba values, which correspond to altered Ca–Sr patterns in some wells (Figure 6).

Although these issues were mitigated through systematic washing (Figure 2A), barite quantification (Figure 8), duplicate analyses (Figure 3A–B), and cross-validation with XRD mineralogical data, they cannot be fully eliminated. The marked improvement in Ca–Sr correlation after outlier removal (Table 4; Figure 10) further underscores the relevance of filtering strategies to recover primary geochemical signals.

Despite these constraints, the consistent separation of Ca and Sr curves between the Itapema and Barra Velha formations across multiple wells (figures 11 and 12) demonstrates that the method remains robust and operationally effective. This reinforces the applicability of real-time XRF and XRD analyses as practical tools for identifying the Pre-Alagoas Unconformity under field conditions, even within the inherent limitations of rig-based workflows.

5. CONCLUSION

- The Ca–Sr trend method proved effective for identifying the unconformity between the Barra Velha and Itapema formations during drilling operations using XRF analyses of cuttings samples.

- The Ca-Sr ratio serves as a robust stratigraphic discriminator between the Barra Velha and Itapema formations, reflecting differences in paleosalinity and carbonate precipitation dynamics.
- Assessment of barite contamination is essential before applying the method. Contamination levels above 10% compromise data reliability and may lead to misinterpretation.
- Barite contamination affects XRF results but does not impact XRD analyses. This influence is linked to the efficiency of washing procedures and the reduction of barite from samples.
- Silicification and hydrothermal dolomitization further alter the geochemical signal, as strontium is a mobile element and may be remobilized under such conditions.
- Integrating XRF and XRD analyses enhances formation characterization, providing cross-validation between geochemical and mineralogical data and improving interpretability in real-time geological operations.
- Applying statistical filtering and outlier removal improves dataset reliability, clarifying the Ca–Sr relationship by mitigating the effects of drilling-related contamination and diagenetic overprint.

REFERENCES

Abdou, M.I., Al-Sabagh, A.M., El-Ahmed, A.M.H., and Fadl, A.M., 2018, Impact of barite and ilmenite mixture on enhancing the drilling mud weight: Egyptian Journal of Petroleum, v. 27, p. 955–967, doi: https://doi.org/10.1016/j.ejpe.2018.02.004.

Altenhofen, S.D., Rodrigues, A.G., Borghi, L., and De Ros, L.F., 2024, Dynamic re-sedimentation of lacustrine carbonates in the Búzios Field, pre-salt section of Santos Basin, Brazil: Journal of South American Earth Sciences, v. 138, doi: https://doi.org/10.1016/j.jsames.2024.104863.

Amorim, J.C., Vidal, F., Freire, A.F.M., Florenzano, R.C., Borges, K.I.M., and Salgado-Campos, V.M.J., 2024, Caracterização mineralógica, litogeoquímica e geofísica da formação Piçarras, bacia de Santos, a partir de perfis de poços e amostras de calha, *in* Congresso Brasileiro de Geologia, 51°, Minas Gerais: Belo Horizonte, Brasil.

Andrews, M.G., and Jacobson, A.D., 2017, The radiogenic and stable Sr isotope geochemistry of basalt weathering in Iceland: Role of hydrothermal calcite and implications for long-term climate regulation: Geochimica et Cosmochimica Acta, v. 215, p. 247-262, doi: https://doi.org/10.1016/j.gca.2017.08.012.

Araújo, C.C., Madrucci, V., Moretti Júnior, P.A., Silva Filho, R.P., Spadini, A.R., Homewood, P., Mettraux, M., and Ramnani, C.W., 2024, Estratigrafia e modelos deposicionais carbonáticos do Pré-sal da Bacia de Santos, *in* Chagas, A.A.P., Araújo, C.C., and Santos, L.A., eds., As grandes descobertas do Pré-sal no Atlântico Sul, Brasil, Rio de Janeiro: Petrobras, p. 471-565.

Bahr, A., Lamy, F., Arz, H.W., Major, C., Kwiecien, O., and Wefer, G., 2008, Abrupt changes of temperature and water chemistry in the late Pleistocene and early Holocene Black Sea: Geochemistry, Geophysics, Geosystems, v. 9, n. 1, doi: https://doi.org/10.1029/2007GC001683.

Basso, M., Belila, A.M.P., Chinelatto, G.F., Souza, J.P.D.P., and Vidal, A.C., 2021, Sedimentology and petrophysical analysis of pre-salt lacustrine carbonate reservoir from the Santos Basin, southeast Brazil: International Journal of Earth Sciences, v. 110, p. 2573-2595, doi: https://doi.org/10.1007/s00531-020-01932-7.

Bourgoyne Jr., A.T., Millheim, K.K., Chenevert, M.E., and Young Jr., F.S., 1986, Applied Drilling Engineering: Society of Petroleum Engineers, 544 p.

Carvalho, A.M.A., Hamon, Y., De Souza Jr, O.G., Carramal, N.G., and Collard, N., 2022, Facies and diagenesis distribution in an Aptian pre-salt carbonate reservoir of the Santos Basin, offshore Brazil: a comprehensive quantitative approach: Marine and Petroleum Geology, n. 141, doi: https://doi.org/10.1016/j.marpetgeo.2022.105708.

Chinelatto, G.F., Belila, A.M.P., Basso, M., Souza, J.P.P., and Vidal, A.C., 2020, A taphofacies interpretation of shell concentrations and their relationship with petrophysics: a case study of Barremian-Aptian coquinas in the Itapema Formation, Santos Basin-Brazil: Marine and Petroleum Geology, v. 116, doi: https://doi.org/10.1016/j.marpetgeo.2020.104317.

Chivas, A.R., De Deckker, P., and Shelley, J.M.G., 1985, Strontium content of ostracods indicates lacustrine palaeosalinity: Nature, v. 316, p. 251-253, doi: https://doi.org/10.1038/316251a0.

Craigie, N., 2018, Geochemistry and mineralogy, in Craigie, N., Principles of elemental chemostratigraphy: a practical user guide, p. 39-83, doi: https://doi.org/10.1007/978-3-319-71216-1

Ellis, D.V., and Singer, J.M., 2008, Well logging for earth scientists, Dordrecht: Springer: v. 692.

Gagan M.K., Ayliffe, L.K., Hopley, D., Cali, J.A., Mortimer, G.E., Chappell, J., McCulloch, M.T., and Head, M.J., 1998, Temperature and surface-ocean water balance of the mid-holocene tropical western pacific: Science, v. 279, p. 1014-1018, doi: https://doi.org/10.1126/science.279.5353.1014.

Gomes, J.P., Bunevich, R.B., Tedeschi, L.R., Tucker, M.E., and Whitaker, F.F., 2020, Facies classification and patterns of lacustrine carbonate deposition of the Barra Velha Formation, Santos Basin, Brazilian Pre-salt: Marine and petroleum geology, v. 113, doi: https://doi.org/10.1016/j.marpetgeo.2019.104176.

Gonzaga, H.M., Novo, T.A., da Silva, J.T.G., Boa, T.M.R.F., Gonçalves, L.C., and Cordeiro, M.S., 2024, Stratigraphy and drilling geomechanics of a thick salt section: The Ariri Formation in the eastern portion of the Santos Basin: Journal of South American Earth Sciences, v. 135, doi: https://doi.org/10.1016/j.jsames.2024.104802.

Herlinger Jr, R., Freitas, G.D.N., Anjos, C.D.W., and De Ros, L.F., 2020, Petrological and petrophysical implications of magnesian clays in Brazilian pre-salt deposits, *in* SPWLA Annual Logging Symposium, 61 st.

Herlinger Jr, R., Zambonato, E.E., and De Ros, L.F., 2017, Influence of diagenesis on the quality of Lower Cretaceous pre-salt lacustrine carbonate reservoirs from northern Campos Basin, offshore Brazil: Journal of Sedimentary Research, v. 87, p. 1285-1313, doi: https://doi.org/10.2110/jsr.2017.70.

Hubbard, C.R., and Snyder, R.L., 1988, RIR-measurement and use in quantitative XRD: Powder Diffraction, v. 3, n. 2, p. 74-77, doi: https://doi.org/10.1017/S0885715600013257.

Imbuzeiro, B.M., Vidal, F., Rocha, B.D.S.N., Silveira, C.S., Lupinacci, W.M., Salgado-Campos, V., and Freire, A.F.M., 2024, An integrated approach to characterize diabase sills in Parnaíba Basin, based on geochemical data, cuttings description, and well logs interpretation: Journal of South American Earth Sciences, v. 151, doi: https://doi.org/10.1016/j.jsames.2024.105263.

Imbuzeiro, B.M., 2021, Caracterização de eletrofacies e quimiofacies em soleiras de diabásio da bacia do Parnaíba [Trabalho de Conclusão de curso]: Niteroi, RJ, Universidade Federal Fluminense.

Jesus, I.L.D., Abrantes Jr, F.R., Ferreira, D.J.A., and Lupinacci, W.M., 2023, Carbonate reservoir quality and permoporosity obliteration due to silicification processes in the Barra Velha Formation, Santos Basin, Southeastern Brazil: Brazilian Journal of Geology, v. 53, n. 2, doi: https://doi.org/10.1590/2317-4889202320220086.

Kaur, M., and Singh, D., 2024, Use of EDXRF and WDXRF techniques for trace element analysis: A review *in* AIP Conference Proceedings, 14th v. 2986, p. 030123, https://doi.org/10.1063/5.0193317.

Langer, G., Geisen, M., Baumann, K. H., Kläs, J., Riebesell, U., Thoms, S., Young, J., 2006, Seawater carbonate chemistry, growth rate and processes during experiments with Coccolithus pelagicus and Calcidiscus leptoporus: PANGAEA, doi: https://doi.org/10.1594/PANGAEA.721107. Supplement to: Langer, G. et al., 2006, Species-specific responses of calcifying algae to changing seawater carbonate chemistry: Geochemistry, Geophysics, Geosystems, v. 7, doi: https://doi.org/10.1029/2005GC001227.

Leite, C.O.N., Silva, C.M.A., and De Ros, L.F., 2020, Depositional and diagenetic processes in the pre-salt rift section of a Santos Basin area, SE Brazil: Journal of Sedimentary Research, v. 90, n. 6, p. 584-608, doi: https://doi.org/10.2110/jsr.2020.27.

Leon, J.A.D.L., Penteado, H.L.D.B., Ellis, G.S., Milkov, A., and Mendonça Filho, J.G., 2024, Recognition of Artificial Gases Formed during Drill-Bit Metamorphism Using Advanced Mud Gas: Energies, v. 17, p. 4383, doi: https://doi.org/10.3390/en17174383.

Mohamed, A., Basfar, S., Elkatatny, S., and Al-Majed, A., 2019, Prevention of barite sag in oil-based drilling fluids using a mixture of barite and ilmenite as weighting material: Sustainability, v. 11, n. 20, doi: https://doi.org/10.3390/su11205617.

Moreira, J.L.P., Madeira, C.V., Gil, J.A., and Machado, M.A.P., 2007, Bacia de Santos: Boletim de Geociências da Petrobras, v. 15, n. 2, p. 531-549.

Netto, P. R., Pozo, M., da Silva, M. D., Gomes, M. E. B., Mexias, A., Ramnani, C. W., and Rios-Netto, A.D.M., 2022a, Paleoenvironmental implications of authigenic magnesian clay formation sequences in the Barra Velha Formation (Santos Basin, Brazil): Minerals, v. 12, n. 2, p. 200, doi: https://doi.org/10.3390/min12020200.

Netto, P.R.A., Pozo, M., Silva, M.D., Mexias, A.S., Gomes, M.E.B., Borghi, L., and Rios-Netto, A.M., 2022b, Authigenic Mg-clay assemblages in the Barra Velha Formation (Upper Cretaceous) from Santos Basin (Brazil): The role of syngenetic and diagenetic process: Applied Clay Science, v. 216, doi: https://doi.org/10.1016/j.clay.2021.106339.

Oliveira, F.V.C.S.R.S., et al., 2024, Characterization of subaerial lava flows of the presalt strata in the Santos Basin based on basic well logs: Journal of South American Earth Sciences, v. 139, doi: https://doi.org/10.1016/j.jsames.2024.104884.

Oliveira, F. V. S. R. S., Gomes, R. T. M., Calonio, L. W., Silva, K. M. S., de Oliveira Carmo, I., Bittencourt, B. T., ... & Freire, A. F. M., 2022a, Igneability feature: an effective, easy and low-cost way to identify basic igneous rocks using wireline well logs in open hole wells: Brazilian Journal of Geophysics, v. 40, n. 1, p. 19-41, doi: http://dx.doi.org/10.22564/brjg.v40i1.2156.

Oliveira, F.V.C.S.R.S., Gomes, R.T.M., Roriz, C.E.D., Silva, K.M.S., and Toledo, R.C., 2022b, Lithology Identification Through X-Ray Fluorescence (XRF) Analyses on Drill Cuttings While Drilling, in Santos Basin, *in* SPE Annual Technical Conference and Exhibition, Houston, Texas, USA doi: https://doi.org/10.2118/210151-MS.

Penna, R., Araújo, S., Geisslinger, A., Sansonowski, R., Oliveira, L., Rosseto, J., and Matos, M., 2019, Carbonate and igneous rock characterization through reprocessing, FWI imaging, and elastic inversion of a legacy seismic data set in Brazilian presalt province: The leading edge, v. 38, n. 1, p. 11-19, doi: https://doi.org/10.1190/tle38010011.1.

Pessanha, S., Guilherme, A., and Carvalho, M.L., 2009, Comparison of matrix effects on portable and stationary XRF spectrometers for cultural heritage samples: Applied Physics A, v. 97, p. 497–505, doi: https://doi.org/10.1007/s00339-009-5251-x.

Pietzsch, R., Tedeschi, L.R., Oliveira, D.M., Anjos, C.W.D., Vazquez, J.C., and Figueiredo, M.F., 2020, Environmental conditions of deposition of the Lower Cretaceous lacustrine carbonates of the Barra Velha Formation, Santos Basin (Brazil), based on stable carbon and oxygen isotopes: a continental record of pCO2 during the onset of the Oceanic Anoxic Event 1a (OAE 1a) interval?: Chemical Geology, v. 535, doi: https://doi.org/10.1016/j.chemgeo.2019.119457.

Ramos, G.O., 2022, Avaliação do potencial da formação pimenteiras para reservatórios não convencionais do tipo shale-gas no poço 1-OGX-101-ma, área do Parque dos Gaviões, bacia do Parnaíba [Trabalho de Conclusão de curso]: Niteroi, RJ, Universidade Federal Fluminense.

Ribeiro, D.S.T., 2019, Estudo de razões de compostos químicos para análises paleoambientais na Formação Codó, com base em amostras de calha de poços do Parque dos Gaviões, Bacia do Parnaíba [Dissertação de Mestrado]: Niteroi, RJ, Universidade Federal Fluminense.

Ribeiro, L.F., (2021). Interpretação paleoambiental e paleodeposicional da formação Poti com base em proxies geoquímicas, na área do Parque dos Gaviões, bacia do Parnaíba [Trabalho de Conclusão de curso]: Niteroi, RJ, Universidade Federal Fluminense.

Rocha, B.S., 2024, Interpretação de padrões deposicionais lacustres a partir de perfis de raios gama e amostras de calha na formação Codó, Aptiano da bacia do Parnaíba [Trabalho de Conclusão de curso]: Niteroi, RJ, Universidade Federal Fluminense.

Rollinson, H.R., Rollinson, H., and Pease, V., 2021, Using geochemical data: to understand geological processes, Cambridge University Press.

Rubim, I., Gonçalves, L., Correia, S., Martins, L., Souza, A., and Lima, F., 2024, Silicification Impacts on the Drilling of Pre-Salt Carbonate Reservoirs (Santos Basin–SE Brazil), *in* EAGE Annual Conference & Exhibition (including the Workshop Programme), 85th, European Association of Geoscientists & Engineers, v. 2024, n. 1, p. 1-5.

Saibro, M.B., 2021, Interpretação paleodeposicional e paleoambiental da formação Codó com base em quimioestratigrafia, na área do Parque dos Gaviões – bacia do Parnaíba [Trabalho de Conclusão de curso]: Niteroi, RJ, Universidade Federal Fluminense.

Sartorato, A.C.L., Tonietto, S.N., and Pereira, E., 2020, Silicification and dissolution features in the brazilian Pre-salt Barra Velha formation: impacts in the reservoir quality and insights for 3D geological modeling, *in* Rio Oil & Gas Expo and Conference, Brazil: Rio de Janeiro.

Silva, M.D., Gomes, M.E.B., Mexias, A.S., et al., 2021, Mineralogical study of levels with magnesian clay minerals in the Santos Basin, aptian pre-salt Brazil: Minerals, v.11, n. 9, p. 970, doi: https://doi.org/10.3390/min11090970.

Tang, J., Dietzel, M., Böhm, F., Köhler, S.J., and Eisenhauer, A., 2008b, Sr^{2+}/Ca^{2+} and $^{44}Ca/^{40}Ca$ fractionation during inorganic calcite formation: II. Ca isotopes: Geochimica et Cosmochimica Acta, v. 72, p. 3733–3745, doi: https://doi.org/10.1016/j.gca.2008.05.033.

Tang, J., Köhler, S.J., Dietzel, M., 2008a, Sr^{2+}/Ca^{2+} and $^{44}Ca/^{40}Ca$ fractionation during inorganic calcite formation: I. Sr incorporation: Geochimica et Cosmochimica Acta, v. 72, p. 3718–3732, doi: https://doi.org/10.1016/j.gca.2008.05.031.

Tang, J., Niedermayr, A., Köhler, S.J., Böhm, F., Kısakürek, B., Eisenhauer, A., Dietzel, M., 2012, Sr^{2+}/Ca^{2+} and $^{44}Ca/^{40}Ca$ fractionation during inorganic calcite formation: III. Impact of salinity/ionic strength: Geochimica et Cosmochimica Acta, v. 77, p. 432-443, doi: https://doi.org/10.1016/j.gca.2011.10.039.

Terra, S.A., Silva, D.R.L., Ribeiro, A., and Borghi, L., 2023, The lower Barra Velha formation (Aptian) in the Atapu field, Santos basin: Geological model for a pre-salt succession: Journal of South American Earth Sciences, v. 131, doi: https://doi.org/10.1016/j.jsames.2023.104589.

Wright, V. P., and Barnett, A. J., 2020, The textural evolution and ghost matrices of the Cretaceous Barra Velha Formation carbonates from the Santos Basin, offshore Brazil: Facies, v. 66, n. 7, doi: https://doi.org/10.1007/s10347-019-0591-2.

Yu, G., Chen, J., Xue, C., Chen, Y., Chen, F., and Du, X., 2009, Geochronological framework and Pb, Sr isotope geochemistry of the Qingchengzi Pb–Zn–Ag–Au orefield, Northeastern China: Ore Geology Reviews, v. 35, n. 3-4, p. 367-382, doi: https://doi.org/10.1016/j.oregeorev.2008.11.009.